Quantum Coherent Tunable Coupling of Superconducting Qubits

A. O. Niskanen, *et al.*

Science **316**, 723 (2007);
DOI: 10.1126/science.1141324

Science (print ISSN 0036-8075; online ISSN 1095-9203) is published weekly, except the last week in December, by the American Association for the Advancement of Science, 1200 New York Avenue NW, Washington, DC 20005.

4. K. Piotrowska, M. Zernicka-Goetz, *Development* **129**, 5803 (2002).
5. K. Piotrowska, M. Zernicka-Goetz, *Nature* **409**, 517 (2001).
6. R. L. Gardner, *Development* **128**, 839 (2001).
7. B. Plusa *et al.*, *Nature* **434**, 391 (2005).
8. N. Motosugi, T. Bauer, Z. Polanski, D. Solter, T. Hiiragi, *Genes Dev.* **19**, 1081 (2005).
9. V. B. Alarcon, Y. Marikawa, *Biol. Reprod.* **69**, 1208 (2003).
10. V. B. Alarcon, Y. Marikawa, *Mol. Reprod. Dev.* **72**, 354 (2005).
11. A. Chroscicka, S. Komorowski, M. Maleszewski, *Mol. Reprod. Dev.* **68**, 308 (2004).
12. T. Fujimori, Y. Kurotaki, J. Miyazaki, Y. Nabeshima, *Development* **130**, 5113 (2003).
13. M. Waksmundzka, A. Wisniewska, M. Maleszewski, *Biol. Reprod.* **75**, 582 (2006).
14. H. Niwa *et al.*, *Cell* **123**, 917 (2005).
15. D. Strumpf *et al.*, *Development* **132**, 2093 (2005).
16. T. P. Fleming, *Dev. Biol.* **119**, 520 (1987).
17. A. H. Handyside, *J. Embryol. Exp. Morphol.* **45**, 37 (1978).
18. M. H. Johnson, C. A. Ziomek, *Cell* **24**, 71 (1981).
19. A. K. Tarkowski, J. Wroblewska, *J. Embryol. Exp. Morphol.* **18**, 155 (1967).
20. T. Kanda, K. F. Sullivan, G. M. Wahl, *Curr. Biol.* **8**, 377 (1998).
21. P. Soriano, *Nat. Genet.* **21**, 70 (1999).
22. K. Piotrowska-Nitsche, M. Zernicka-Goetz, *Mech. Dev.* **122**, 487 (2005).
23. R. L. Gardner, T. J. Davies, *Hum. Reprod.* **21**, 492 (2006).
24. R. L. Gardner, *Development* **124**, 289 (1997).
25. Materials and methods are available on *Science* Online.
26. H. Tsutsui, S. Karasawa, H. Shimizu, N. Nukina, A. Miyawaki, *EMBO Rep.* **6**, 233 (2005).
27. K. Hatta, H. Tsuji, T. Omura, *Nat. Protoc.* **1**, 960 (2006).
28. R. L. Gardner, *Hum. Reprod.* **22**, 798 (2007).
29. R. L. Gardner, T. J. Davies, *Hum. Reprod.* **17**, 1839 (2002).
30. D. Gray *et al.*, *Curr. Biol.* **14**, 397 (2004).
31. Contact K.H. (khatt@sci.u-hyogo.ac.jp) for CAG-KikGR-1 mouse. The authors acknowledge the members of the animal facility for the care of the mice used in this study, S. Yoshida for critical reading of the manuscript, and S. Aizawa for encouragement. We thank the LARGE in CDB, RIKEN for providing the CAG-KikGR-1 transgenic mouse (CDB0201T) and P. Soriano for providing genomic DNA fragments of the Rosa26 locus. This work was initiated with support from PRESTO (Precursory Research for Embryonic Science and Technology), JST, and supported by grants-in-aid for scientific research from Ministry of Education, Culture, Sports, Science, and Technology of Japan.

Supporting Online Material

www.sciencemag.org/cgi/content/full/1138591/DC1
Materials and Methods
SOM Text
Figs. S1 to S3
Movies S1 and S2

8 December 2006; accepted 21 March 2007
Published online 19 April 2007;
10.1126/science.1138591
Include this information when citing this paper.

Quantum Coherent Tunable Coupling of Superconducting Qubits

A. O. Niskanen,[1,4] K. Harrabi,[1] F. Yoshihara,[2] Y. Nakamura,[1,2,3]* S. Lloyd,[5] J. S. Tsai[1,2,3]

To do large-scale quantum information processing, it is necessary to control the interactions between individual qubits while retaining quantum coherence. To this end, superconducting circuits allow for a high degree of flexibility. We report on the time-domain tunable coupling of optimally biased superconducting flux qubits. By modulating the nonlinear inductance of an additional coupling element, we parametrically induced a two-qubit transition that was otherwise forbidden. We observed an on/off coupling ratio of 19 and were able to demonstrate a simple quantum protocol.

Macroscopic quantum coherence of superconducting structures is an intriguing physical phenomenon. The reasons for studying it include not only the prospect of constructing a quantum computer but also the possibility of realizing quantum-mechanical coherence in artificially fabricated structures. The properties of superconducting qubits (*1*–*3*) are being vigorously studied, with the relevant coherence times of the quantum states now extending to the microsecond range (*4*–*7*), in particular because the qubits are being operated at optimal bias points (*4*). When two or more qubits are coupled, quantum mechanics predicts that the combination can be, roughly speaking, more than the sum of its constituents. This entirely nonclassical concept is called entanglement. The existing quantum algorithms rely heavily on the use of entangled states. With tunable couplings between individual qubits, the design of control pulses for even a large set of qubits is relatively straightforward because the system can be divided into small noninteracting blocks. With nontunable couplings, as in nuclear magnetic resonance quantum computing, a large fraction of the quantum operations performed has to be devoted to effective decoupling procedures (*8*). Recently, several experiments on coupled superconducting qubits have been carried out with both fixed (*9*–*15*) and tunable (*16*–*18*) coupling. Unfortunately, most coupling schemes for superconducting qubits are efficient only away from the optimal point, which results in a shorter coherence time. Thus, realizing tunable coupling at the coherence optimal bias point is crucial for future scalability.

We studied superconducting flux qubits (*19*), which are superconducting loops interrupted by Josephson junctions. When a magnetic flux Φ_j close to half-flux quantum $\Phi_0/2$ is applied through the loop of qubit j, the two lowest-energy states have the supercurrents $\pm I_{pj}$ rotating in opposite directions. The magnetic energy difference $\varepsilon_j = 2I_{pj}(\Phi_j - \Phi_0/2)$ between these states can be controlled via Φ_j. The tunnelling energy between the states is Δ_j. The qubit states have eigenenergies $\pm\omega_j/2$, where $\omega_j = \sqrt{\{\Delta_j^2 + \varepsilon_j^2\}}$, as shown schematically in Fig. 1A. Resonant control of qubits is possible by modulating ε_j at the frequency ω_j. At the flux optimal point $\Phi_j = \Phi_0/2$, the eigenstates are equal superpositions of the circulating current states, and therefore the expectation value of current vanishes. At this point, the quantum coherence is found to be far superior (*6*, *7*) to the case where $\Phi_j \neq \Phi_0/2$, because $d\omega_j/d\Phi_j = 0$ and thus the accumulated quantum phase proportional to the time integral of ω_j is insensitive to flux noise.

The natural coupling between qubits k and l is via mutual inductance $M_{kl} > 0$, resulting in the antiferromagnetic coupling $J_{kl} = M_{kl}I_{pk}I_{pl}$. A collection of n qubits can be described by the Hamiltonian

$$H = -\frac{1}{2}\sum_{j=1}^{n}(\Delta_j\sigma_z^j + \varepsilon_j\sigma_x^j) + \sum_{k=1}^{n}\sum_{l=k+1}^{n} J_{kl}\sigma_x^k\sigma_x^l \quad (1)$$

where σ_x^j and σ_z^j are Pauli matrices operating on qubit j. Owing to vanishing persistent currents (or the off-diagonal coupling term), the coupling only has a weak second-order effect at the optimal point ($\varepsilon_k = \varepsilon_l = 0$) if $J_{kl} \ll |\Delta_k - \Delta_l|$. It is thus easy to decouple qubits at the optimal point. To realize universal two-qubit gates (that is, to turn the coupling on), it would be ideal to drive either the $|00\rangle \leftrightarrow |11\rangle$ or the $|10\rangle \leftrightarrow |01\rangle$ transition, where $|jk\rangle$ are the two-qubit eigenstates. This results in a gate equally as efficient as the controlled-NOT (CNOT). However, simply driving the fluxes Φ_1 and Φ_2 with microwaves in resonance with such transitions cannot realize the desired operation because the microwave essen-

[1]CREST, Japan Science and Technology Institute, Kawaguchi, Saitama 332-0012, Japan. [2]The Institute of Physical and Chemical Research (RIKEN), Wako, Saitama 351-0198, Japan. [3]NEC Fundamental and Environmental Research Laboratories, Tsukuba, Ibaraki 305-8501, Japan. [4]VTT Technical Research Centre of Finland, Sensors, Post Office Box 1000, 02044 VTT, Finland. [5]Massachusetts Institute of Technology, Cambridge, MA 02139, USA.

*To whom correspondence should be addressed. E-mail: yasunobu@ce.jp.nec.com

tially couples through single-qubit operators σ_x^j. In general, the corresponding transitions are forbidden for any value of J_{kl}, although the eigenstates are modified. Different ways to overcome this problem are being pursued (*20*–*23*).

Our approach (*22*) is to couple two qubits via a third adiabatic qubit ($n = 3$) with higher Δ_3, which results in an effective coupling between qubits 1 and 2 given by

$$J_{12}^{\text{eff}} \approx \left(M_{12} + \frac{M_{13}M_{23}}{L_Q}\right) I_{p1} I_{p2} = J_{12} - \frac{2J_{23}J_{13}\Delta_3^2}{\omega_3^3} \quad (2)$$

The coupling can be interpreted as a sum of direct inductive coupling J_{12} and indirect coupling via the nonlinear ground-state inductance $L_Q = -2(d^2\omega_3/d\Phi_3^2)^{-1}$ of qubit 3. Applying a microwave through the loop of qubit 3 at the frequency $(\Delta_2 \mp \Delta_1)/h$ modulates L_Q via ω_3 and results in a term proportional to $\sigma_x^1\sigma_x^2 \pm \sigma_y^1\sigma_y^2$ in the rotating frame for which the desired transitions are allowed. The induced coupling can be thus attributed to the parametric modulation of the coupling energy at a microwave frequency. In the linear approximation, the two-qubit oscillations have the frequency $\Omega_{12}/h = (dJ_{12}^{\text{eff}}/d\varepsilon_3)\delta\varepsilon_3/h$, where $\delta\varepsilon_3$ is the amplitude of the microwave driving applied to qubit 3. This has a maximum around $\varepsilon_3 = \pm\Delta_3/2$ and vanishes at $\varepsilon_3 = 0$ and at $|\varepsilon_3| >> \Delta_3$. We focus here on the sum-frequency transition $|00\rangle \leftrightarrow |11\rangle$. The functioning of the tunable parametric coupling is very convenient. When the microwave at the sum frequency is off, the coupling is also off. Vice versa, when the microwave is turned on, the coupling goes on. The reduced two-qubit rotating-frame Hamiltonian

$$H_{\text{rot}} = \sum_{j=1}^{2} \frac{\Omega_j}{2}(\cos\phi_j\sigma_x^j - \sin\phi_j\sigma_y^j) + \frac{\Omega_{12}}{4}(\sigma_x^1\sigma_x^2 - \sigma_y^1\sigma_y^2) \quad (3)$$

where Ω_j is the (resonant) microwave-induced single-qubit Rabi frequency of qubit j and ϕ_j is the microwave phase, offers full control and can in principle be set to zero by turning off all microwaves.

Figure 1 describes our experimental setup. By using the kinetic inductance of shared superconducting wires, we couple two qubits ($\Delta_1 < \Delta_2$) to a third qubit with a larger gap Δ_3. Direct coupling J_{12} is expected to be small. On the basis of a series of spectroscopic measurements (*24*), we know that we can rely on the accuracy of lithography and have very similar areas (within ~0.5% difference) of qubits 1 and 2. Therefore, we have $\Phi_1 \approx \Phi_2$ even with a single uniform flux bias, whereas Φ_3 is deliberately offset to have a finite Ω_{12}. We can write $\Phi_j = \Phi_3 + \Delta\Phi_j$, where $\Delta\Phi_j$ ($j = 1,2$) is a small offset. To manipulate the qubits, we apply microwaves of controllable duration via an on-chip microwave line. During the manipulation with the microwaves that are assumed to couple to all loops, we apply a small bias current (a few percent of critical current) through the readout superconducting quantum interference device (SQUID) to fine-tune the biases of both qubits 1 and 2 to be at the optimal point. Figure 2 illustrates the measured spectrum when the minima of the qubit transition frequencies are aligned. Qubits 1 and 2 have

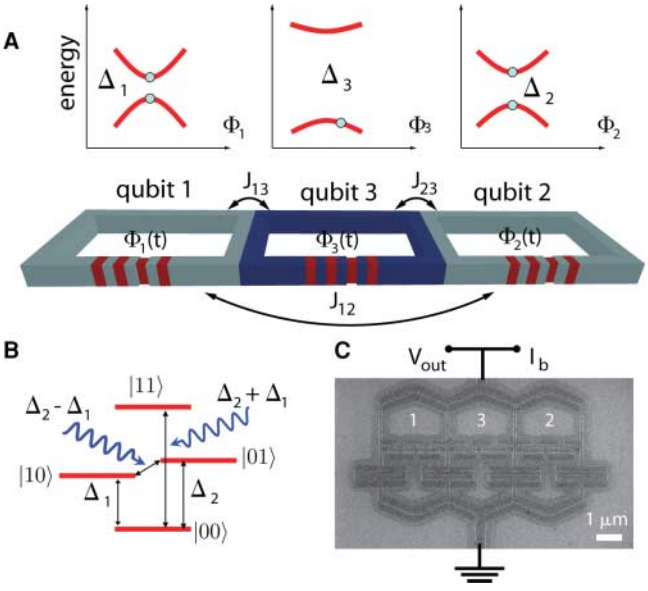

Fig. 1. Schematic of the experiment. (**A**) The system consists of three four-junction flux qubits. In each qubit, one junction is about 0.5 times smaller than others. Qubits 1 and 2 (with energies Δ_1 and Δ_2) are coupled via the kinetic inductance of the shared loop edge to the third. The middle qubit with large Δ_3 is biased slightly away from the half-flux quantum, whereas qubits 1 and 2 are optimally biased. The qubits are controlled via the fluxes $\Phi_j(t)$. (**B**) Level diagram of qubits 1 and 2. Two-qubit operations were carried out using microwaves at either the sum frequency $(\Delta_2 + \Delta_1)/h$ or the difference frequency $(\Delta_2 - \Delta_1)/h$. (**C**) Scanning electron micrograph of the sample fabricated by electron beam lithography and shadow evaporation of aluminum with 20-nm and 35-nm layer thicknesses. The junction oxidation was done with a mixture of Ar and O_2 (90%/10%) at 35 mTorr for 8 min. The qubits couple to a four-junction readout SQUID. When a pulse of the bias current I_b is applied to the SQUID, the probability of switching to the voltage state (monitored via V_{out}) depends on the state of the qubit system. The on-chip circuitry is similar to the single-qubit experiment reported in (*7*), along with a gold bias resistor and a shunt capacitor for the SQUID. The measurements were made at temperatures around 10 mK in a dilution refrigerator.

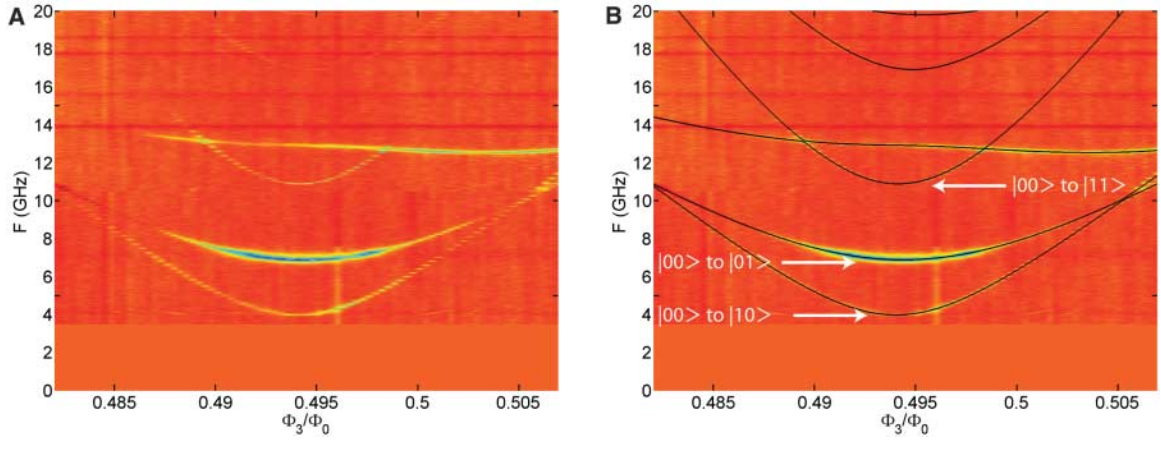

Fig. 2. Large-scale spectrum of the three-qubit system. (**A**) Measured spectrum as a function of flux and frequency (F) from 3.5 to 20 GHz. Blue means a low switching probability, whereas red means a high switching probability. The contrast is at best about 25%. (**B**) The black lines indicate the theoretical spectrum calculated from the three-qubit Hamiltonian. The parameters obtained from the least-squares fitting are $I_{p1}/h = 873 \pm 13$ GHz/Φ_0, $I_{p2}/h = 705 \pm 19$ GHz/Φ_0, $I_{p3}/h = 516 \pm 35$ GHz/Φ_0, $\Delta_1/h = 4.022 \pm 0.078$ GHz, $\Delta_2/h = 6.915 \pm 0.075$ GHz, $\Delta_3/h = 12.454 \pm 0.074$ GHz, $\Delta\Phi_1 = 5.58 \pm 0.11$ mΦ_0, $\Delta\Phi_2 = 5.31 \pm 0.22$ mΦ_0, $J_{12}/h = -0.003 \pm 0.066$ GHz, $J_{13}/h = 0.715 \pm 0.130$ GHz, and $J_{23}/h = 0.482 \pm 0.171$ GHz.

sufficiently different gaps as designed, and a sign of the desired sum-frequency transition is also visible.

To show that the coupling scheme is indeed tunable and coherent, we have to be able to set the rotating-frame Hamiltonian to zero as well as to drive the single-qubit transitions in time domain regardless of the input state (off). Also, we have to be able to drive, in a time domain, the two-qubit transition (on). Figure 3 shows measured examples of this at the combined optimal point of qubits 1 and 2. It is clear that a single-qubit transition frequency does not depend significantly on the state of the other. On the other hand, we can drive the sum-frequency transition as fast as $\Omega_{12}^{max}/h = 23.2$ MHz, which is obtained with the maximum power we can apply with the present microwave source and attenuation of our setup. The minimum time for a universal gate is given by half of the period; that is, 22 ns. A quantitative measure of the on/off ratio is obtained by comparing the maximal two-qubit oscillation frequency to the frequency at which unwanted coupling takes place. Using a Ramsey fringe measurement of the different transitions, we find that the Hamiltonian in the energy eigenbasis (and thus the logical rotating-wave Hamiltonian) has a spurious term $-(\kappa/2)\sigma_z^1\sigma_z^2$, with $\kappa/h = 1.23$ MHz, which is quite small compared to the single-qubit frequencies of about 4.000 GHz and 6.889 GHz. Because this term results in unwanted phase rotation at the frequency κ/h, we conclude that the demonstrated on/off ratio of our coupling scheme is $\Omega_{12}^{max}/\kappa \approx 19$. In addition to the high degree of tunability, the coherence properties are quite good, as characterized by the relaxation time T_1 and the Ramsey dephasing time T_2^{Ramsey}. Qubit 2 has about $T_1 = 1.0$ μs and $T_2^{Ramsey} = 0.8$ μs, whereas qubit 1 has $T_1 = 0.3$ μs and $T_2^{Ramsey} = 0.2$ μs. The lifetime of the state $|11\rangle$ is limited by qubit 1, and we get $T_2^{Ramsey} = 0.2$ μs for the sum-frequency transition. The reduced coherence time of qubit 1 is caused by a resonance close by. The fact that the resonant frequency of the two-qubit transition is reduced at large driving amplitudes can be understood from simulation as the effect of unwanted coupling of the microwave to qubits 1 and 2 (*6*, *25*), which is unavoidable in the present sample design.

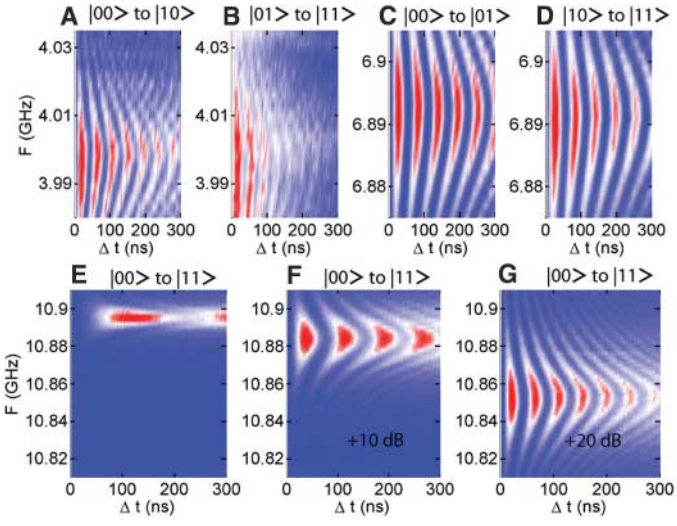

Fig. 3. Examples of single-qubit transitions and the two-qubit operation. (**A** to **D**) Single-qubit Rabi oscillations as a function of microwave frequency and time with different initial states. Δt, change in time. (**A**) and (**B**) illustrate the $|00\rangle \leftrightarrow |10\rangle$ and $|01\rangle \leftrightarrow |11\rangle$ transitions, respectively, both corresponding to qubit 1 but with different initial states of qubit 2. Similarly, (**C**) and (**D**) show the $|00\rangle \leftrightarrow |01\rangle$ and $|10\rangle \leftrightarrow |11\rangle$ transitions of qubit 2. We see that single-qubit resonant frequencies do not depend on the state of the other qubit by more than a couple of megahertz. (**E** to **G**) Examples of the coherent oscillations of the two-qubit $|00\rangle \leftrightarrow |11\rangle$ transitions with three different powers. The applied power increases from (**E**) in steps of 10 dB. The shift of the resonant frequency with higher power is qualitatively explained by simulation to be due to cross-coupling of the microwave to qubits 1 and 2. The visibility in the readout signal in the case of qubit 1 is about 12% and in the case of qubit 2 is about 30%. The sum-frequency transition has a visibility of about 40%. However, the readout is not designed to distinguish between the four possible outcomes. For qubit 1, the visibility and coherence time are reduced by the presence of an unidentified resonance around 4.05 GHz. This may be responsible for the change in Rabi frequency for qubit 1 for different initial states as well.

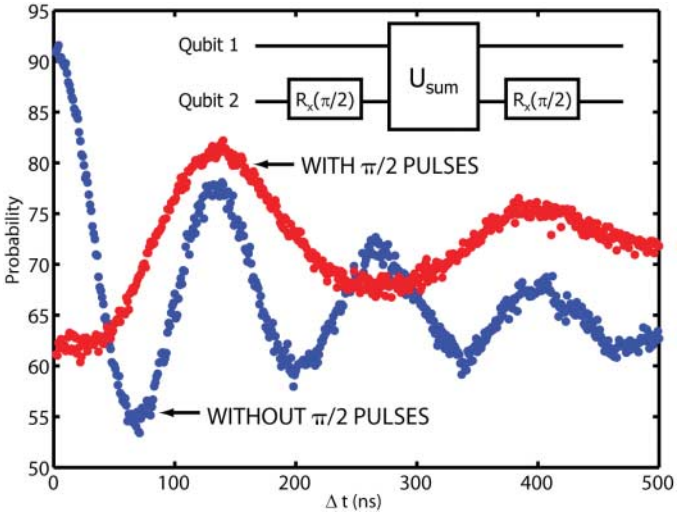

Fig. 4. Example of a simple quantum protocol. The inset at top illustrates the quantum circuit of the protocol for detecting the 4π periodicity of the sum-frequency gate U_{sum}. Here, $R_x(\pi/2)$ stands for the rotation of a qubit around the x axis. Applying the $\pi/2$ pulse on qubit 2 rather than qubit 1 is more practical with the present readout visibilities. The blue curve shows the regular two-qubit coherent oscillations. The red curve shows the result of the protocol with the extra $\pi/2$ pulses. Both measurements were carried out using the same microwave power for the sum frequency. The used microwave frequencies were 10.878 GHz for the sum-frequency transition and 6.889 GHz for qubit 2. The microwave sources were phase-locked together with the chopping pulse. The oscillation period is doubled in the case of the protocol, as expected.

As further proof of the functioning of the scheme and the good coherence properties combined with a high on/off ratio, we have demonstrated a simple multipulse quantum protocol related to quantum coin tossing (*26*). One application of quantum coin tossing is to store classical information in a way that is immune to certain types of intervention and noise. For example, if one stores classical bits on eigenstates of σ_x, then these bits are immune to the action of a malicious quantum hacker who breaks into one's quantum computer and flips bits about the x axis: Because of the coding, the hacker may think he or she is flipping bits but is in fact only applying a global phase to each bit. Our protocol is complementary to this: We detect the presence of a classically benign hacker, who performs an operation whose sole effect is to multiply certain logical states by a phase. Such a phase is classically undetectable: The operation of the benign hacker on classical bits is to apply a global phase. Quantum-mechanically, however, one can detect this hacker by using superposition and entanglement. Figure 4 shows the performance of the protocol.

Driving at the sum-frequency transition induces the unitary gate $U_{sum} = \exp[-i\theta/4(\sigma_x^1\sigma_x^2 - \sigma_y^1\sigma_y^2)]$, where θ is varied by the microwave duration. When $\theta = \pi$, the gate is equivalent to the double-CNOT (or the iSWAP) up to single-qubit rotations. Three applications of this gate suffice to generate any two-qubit gate when supplemented by single-qubit gates (*27*). At $\theta = 2\pi$, the gate is diagonal with the entries $(-1,1,1,-1)$, and if the input state is an eigenstate, the resulting oscillation thus has a 2π period. But the underlying period is actually 4π, which can be revealed

using superposition states. We do this by applying a $\pi/2$ rotation on qubit 2 before and after the application of U_{sum}. The experimental confirmation of this purely quantum-mechanical effect is shown in Fig. 4, where we see that the oscillation frequency is halved and phase-shifted when $\pi/2$ rotations are used. There is no analogy for this effect for a single qubit, because there the phase is just global and undetectable. The measurement result demonstrates the familiar quantum fact that you have to rotate by 4π, not 2π, to get back to where you started and is clear evidence of the entanglement inherent in the correlations between the qubits during their time evolution.

Our experiments demonstrate that the tunable coupling between flux qubits can be realized entirely using the application of microwaves at the coherence optimal point, which is very important for scalability. This indicates that parametric couplers are strong candidates as fundamental building blocks of gate-based quantum computers, but optimization of the scheme requires further study. We expect the coherence time of tunably coupled qubits to reach the same level as that of individual optimized qubits when, for example, independent readouts allowing for bias optimization (*6*, *7*) are combined with this coupling scheme in a future device.

References and Notes

1. Y. Nakamura, Yu. A. Pashkin, J. S. Tsai, *Nature* **398**, 786 (1999).
2. J. M. Martinis, S. Nam, J. Aumentado, C. Urbina, *Phys. Rev. Lett.* **89**, 117901 (2002).
3. I. Chiorescu, Y. Nakamura, C. J. P. M. Harmans, J. E. Mooij, *Science* **299**, 1869 (2003).
4. D. Vion *et al.*, *Science* **296**, 886 (2002).
5. A. Wallraff *et al.*, *Phys. Rev. Lett.* **95**, 060501 (2005).
6. P. Bertet *et al.*, *Phys. Rev. Lett.* **95**, 257002 (2005).
7. F. Yoshihara, K. Harrabi, A. O. Niskanen, Y. Nakamura, J. S. Tsai, *Phys. Rev. Lett.* **97**, 167001 (2006).
8. D. G. Cory *et al.*, *Fortschr. Phys.* **48**, 875 (2000).
9. Yu. A. Pashkin *et al.*, *Nature* **421**, 823 (2003).
10. T. Yamamoto, Yu. A. Pashkin, O. Astafiev, Y. Nakamura, J. S. Tsai, *Nature* **425**, 941 (2003).
11. A. J. Berkley *et al.*, *Science* **300**, 1548 (2003).
12. J. B. Majer, F. G. Paauw, A. C. J. ter Haar, C. J. P. M. Harmans, J. E. Mooij, *Phys. Rev. Lett.* **94**, 090501 (2005).
13. R. McDermott *et al.*, *Science* **307**, 1299 (2005).
14. M. Steffen *et al.*, *Science* **313**, 1423 (2006).
15. M. Grajcar *et al.*, *Phys. Rev. Lett.* **96**, 047006 (2006).
16. S. H. W. van der Ploeg *et al.*, *Phys. Rev. Lett.* **98**, 057004 (2007).
17. R. Harris *et al.*, preprint available at http://arxiv.org/abs/cond-mat/0608253.
18. T. Hime *et al.*, *Science* **314**, 1427 (2006).
19. J. E. Mooij *et al.*, *Science* **285**, 1036 (1999).
20. C. Rigetti, A. Blais, M. Devoret, *Phys. Rev. Lett.* **94**, 240502 (2005).
21. P. Bertet, C. J. P. M. Harmans, J. E. Mooij, *Phys. Rev. B* **73**, 064512 (2006).
22. A. O. Niskanen, Y. Nakamura, J. S. Tsai, *Phys. Rev. B* **73**, 094506 (2006).
23. M. Grajcar, Y. X. Liu, F. Nori, A. M. Zagoskin, *Phys. Rev. B* **74**, 172505 (2006).
24. A. O. Niskanen, K. Harrabi, F. Yoshihara, Y. Nakamura, J. S. Tsai, *Phys. Rev. B* **74**, 220503 (2006).
25. D. I. Schuster *et al.*, *Phys. Rev. Lett.* **94**, 123602 (2005).
26. D. A. Meyer, *Phys. Rev. Lett.* **82**, 1052 (1999).
27. J. Zhang, J. Vala, S. Sastry, K. B. Whaley, *Phys. Rev. A* **69**, 042309 (2004).

28. We thank A. Maassen van den Brink, A. Zagoskin, A. Smirnov, and S. Ashhab for discussions.

14 February 2007; accepted 22 March 2007
10.1126/science.1141324

Beating the Standard Quantum Limit with Four-Entangled Photons

Tomohisa Nagata,[1] Ryo Okamoto,[1,2] Jeremy L. O'Brien,[3,4] Keiji Sasaki,[1] Shigeki Takeuchi[1,2]*

Precision measurements are important across all fields of science. In particular, optical phase measurements can be used to measure distance, position, displacement, acceleration, and optical path length. Quantum entanglement enables higher precision than would otherwise be possible. We demonstrated an optical phase measurement with an entangled four-photon interference visibility greater than the threshold to beat the standard quantum limit—the limit attainable without entanglement. These results open the way for new high-precision measurement applications.

Quantum metrology involves using quantum mechanics to realize more precise measurements than can be achieved with classical methods (*1*). The canonical example uses entanglement of N particles to measure a phase with a precision $\Delta\phi = 1/N$—the Heisenberg limit. Such a measurement outperforms the $\Delta\phi = 1/\sqrt{N}$ precision limit possible with N unentangled particles—the standard quantum limit (SQL). Progress has been made with trapped ions (*2*–*4*) and atoms (*5*, *6*), while high-precision optical phase measurements have many important applications, including microscopy, gravity-wave detection, measurements of material properties, and medical and biological sensing. Although a reduced de Broglie wavelength (*7*) has been reported for three (*8*), four (*9*, *10*), and even six (*11*) photons, the SQL has been beaten only with two photons (*12*–*16*).

We demonstrated an entangled four-photon phase measurement with a visibility that exceeds the threshold to beat the SQL. We used an ultrastable displaced-Sagnac implementation of a scheme with a high intrinsic efficiency to achieve a four-photon interference visibility of 91%. We also demonstrated that measuring a reduced de Broglie wavelength does not mean beating the SQL, in another experiment that shows high-visibility multiphoton fringes, but cannot beat the SQL. The high-precision multiphoton quantum interference demonstrated here is key, not only to quantum metrology and quantum lithography (*14*, *17*, *18*), but also to other optical quantum technologies.

The Heisenberg limit and the SQL can be illustrated with reference to an interferometer (Fig. 1, inset) (*19*–*23*). We represent a single photon in mode a and no photons in mode b by the quantum state $|10\rangle_{ab}$. After the first beam splitter, this photon is in a quantum mechanical superposition of being in both paths of the interferometer: $(|10\rangle_{cd} + |01\rangle_{cd})/\sqrt{2}$. This superposition evolves to the state $(|10\rangle_{cd} + e^{i\phi}|01\rangle_{cd})/\sqrt{2}$ after the ϕ phase shift in mode d. After recombining at the second beam splitter, the probability of detecting the single photon in mode e is $P_e = (1 - \cos\phi)/2$, which can be used to estimate ϕ. If we repeat this experiment N times, then the uncertainty in this estimate is $\Delta\phi = 1/\sqrt{N}$—the SQL. If instead we were able to prepare the maximally entangled N-photon state $(|N0\rangle_{cd} + |0N\rangle_{cd})/\sqrt{2}$ inside the interferometer, this state would evolve to $(|N0\rangle_{cd} + e^{iN\phi}|0N\rangle_{cd})/\sqrt{2}$ after the ϕ phase shift. From this state we could estimate the phase with an uncertainty $\Delta\phi = 1/N$—the Heisenberg limit—an improvement of $1/\sqrt{N}$ over the SQL. Beating the SQL is known as phase supersensitivity (*8*, *11*).

The $N\phi$ dependence of the phase of the maximally entangled state $(|N0\rangle_{cd} + |0N\rangle_{cd})/\sqrt{2}$ is a manifestation of the N-photon de Broglie wavelength λ/N. This dependence can give rise to an interference oscillation N times faster than that of single photons—phase superresolution (*8*, *11*). Observation of this reduced de Broglie wavelength has sometimes been interpreted in the context of beating the SQL. However, it has been shown recently that high-visibility (*24*) λ/N resolution can be observed with a purely classical system (*11*). This demonstrates that phase superresolution by itself does not guarantee a quantum-mechanical advantage. Rather, phase supersensitivity, or beating the SQL, is the most important criterion.

[1]Research Institute for Electronic Science, Hokkaido University, Sapporo 060-0812, Japan. [2]Japan Science and Technology Agency, Honcho, Kawaguchi-shi, Saitama, 332-0012, Japan. [3]Department of Electrical and Electronic Engineering, University of Bristol, Merchant Venturers Building, Woodland Road, Bristol BS8 1UB, UK. [4]H. H. Wills Physics Laboratory, University of Bristol, Tyndall Avenue, Bristol BS8 1TL, UK.

*To whom correspondence should be addressed. E-mail: takeuchi@es.hokudai.ac.jp